*Int. J. Electrochem. Sci.*, 10 **(2015)** 1582 - 1594

International Journal of
ELECTROCHEMICAL
SCIENCE
www.electrochemsci.org

# Few-layer Graphene Prepared Via Microwave Digestion Reduction and its Electrochemical Performances in Lithium Ion Batteries

*Li-lai Liu*[1,2], *Mao-zhong An*[1,*], *Pei-xia Yang*[1], *Jin-qiu Zhang*[1]

[1] School of Chemical Engineering and Technology, Harbin Institute of Technology, Harbin, 150001, China
[2] College of Environmental and Chemical Engineering, Heilongjiang University of Science and Technology, Harbin 150022, China
[*]E-mail: mzan@hit.edu.cn

*Received:* 4 November 2014 / *Accepted:* 12 December 2014 / *Published:* 30 December 2014

A simple approach is proposed to prepare graphene sheets by microwave digestion reduced graphene oxide without any auxiliary reagents. This method is easily controlled and the graphene oxide as graphene precursor is not must be washed to neutral. The materials are characterized by X-ray diffraction, Fourier-transform infrared spectroscopy, Raman spectroscopy, transmission electron microscopy, high resolution transmission electron microscopy and X-ray photoelectron spectroscopy. The electrochemical properties of graphene sheets anode for lithium ion batteries are studied by cyclic voltammetry, electrochemical impedance spectroscopy and galvanostatic charge/discharge. The graphene as an anode material exhibits high capacity and excellent electrochemical performance in lithium ion batteries. The first discharge/charge capacities are 2113.8/1069.3 mA h $g^{-1}$ at current densities of 100 mA $g^{-1}$, and the reversible specific capacities remain 733.3 mA h $g^{-1}$ after 100 cycles. The graphene sheets electrode shows excellent lithium storage properties at large current densities. The possible mechanism preparation is analyzed. The microwave digestion can reduce the reaction activation energy and change reaction kinetics. In this reaction, overheated supercritical water can play the role of reducing agent and offers a green chemistry alternative to organic solvents.

**Keywords:** Graphene sheets, Microwave digestion, Lithium ion batteries, Anode materials

## 1. INTRODUCTION

Graphene, a single honeycomb carbon layer of $sp^2$-bonded carbon materials, has attracted tremendous attention due to its excellent physical and chemical properties, such as its superior electronic conductivity ~6000 S $cm^{-1}$, thermal conductivity, Young's modulus of 1 TPa, ultimate

strength ~130 GPa and high theoretical specific surface area ~2630 $m^2$ $g^{-1}$ [1-5]. Graphene is applied in different fields due to these unique properties, such as field effect transistors [6-7], sensors [8-9], actuators [10], super capacitors [11], solar cells [12], thermoelectric modules [13] and lithium-ion batteries [14]. However, the aggregation and restacking easily occurs between graphene sheets due to strong van der Waals, which affects its applications [15]. Methods such as mico-mechanical exfoliation [16], liquid-phase exfoliation [17-18], reduction of graphene oxide (GO) [19], chemical vapor deposition (CVD) [20], surface segregation [21] and molecular beam epitaxial growth [22] have been developed in order to make suitable graphene layers. Each of the methods has its own set of advantages and disadvantages. The mico-mechanical exfoliation, CVD and molecular beam epitaxial growth methods can prepare mono-layered and few-layered graphene with few defects and realize the preparation of graphene with homogenous layer numbers. However, the large-scale applications by above three kinds of methods are difficult to achieve due to their low productivity and high cost [23-24]. Liquid-phase exfoliation and surface segregation is long reaction duration and the fine control of number and structure of graphene sheets over an entire substrate remains a major challenge [25]. A strategy is to decrease the attraction between adjacent layers by expanding the interlayer distance through oxidation or chemical intercalation. This strategy can reduce the van der Waals force significantly, because the force is inversely proportional to the interlayer spacing [26]. GO as a well-known graphene precursor, is a $sp^3$ carbon atoms graphene sheet containing various oxygen functional groups on the surface, edge plane or defect sites, such as hydroxyl, carboxyl, carbonyl and epoxide moieties. The expanded interlayer spacing of GO facilitates the exfoliation significantly [27]. While in comparison, GO has two important characteristics: (1) it can be produced using inexpensive graphite as raw material by cost-effective chemical methods with a high yield, and (2) it is highly hydrophilic and can form stable aqueous colloids to facilitate the assembly of macroscopic structures by simple and cheap solution processes, both of which are important to the large-scale uses of graphene. Reduced GO is more facilely and most widely used in various electrochemical energy technologies.To recover the $sp^2$ carbon graphene, most of the oxygen functional groups have to be removed. The thermal or chemical exfoliation based on GO is more appealing. It is generally believed that these exfoliation approaches are essential for the removal of oxygen-containing moieties. However, the chemical exfoliation always employs extra agents, such as hydrazine [28], $NaBH_4$ [29], hydroquinone [30] and ascorbic acid [31]. Many of these reducing reagents are toxic, corrosive and the reaction requires a long time, and not suitable for large-scale implementation [32]. The thermal method necessarily requires special atmosphere (ultra-high vacuum, Ar, $H_2$), and/or rapid heating ($>$200 ℃ $min^{-1}$) up to 1050 ℃ under Ar gas or up to 800 ℃ under $H_2$ gas [24]. Therefore, it is still significant to prepare graphene sheets by a facile method.

**There are many reports on the synthesis of graphene prepared by microwave irradiation, however these methods need auxiliary reagents [33-35]. In this study, GO is prepared by a two-step oxidation method using large flake graphite as raw material, and graphene is prepared by a microwave digestion reduced graphene oxide. This method is easily controlled and without any auxiliary reagents, and the graphene oxide as graphene precursor is not must be washed to neutral. The electrochemical properties of graphene sheets anode for lithium-ion batteries are studied. The possible mechanism preparation is analyzed.**

## 2. EXPERIMENTAL

### *2.1 Preparation of expanded graphite*

**10 g large flake graphite was added to a 500 mL beaker, followed by 20 mL sulfuric acid (98%) and stirred for 30 min in ice-water; Potassium permanganate (1 g) was added slowly and stirred for 60 min in a water bath at 40 ℃; The mixture was filtered and washed with deionized water until the pH value was 7; Dried at 60 ℃ and expanded at 950 ℃.**

### *2.2 Preparation of graphene oxide*

GO was prepared by a modified Hummer's method. Briefly, 2 g expanded graphite was added to a 500 mL beaker, then added 150 mL concentrated sulfuric acid; the beaker was then placed in an ice-water bath and stirred for 10 min. Potassium permanganate (8 g) was added slowly and stirred for 30 min, then the beaker was placed in a water bath of 35 ℃ and stirred with a mechanical stirrer for 24 h. Deionized water (100 mL) was added to the beaker at 98 ℃ and stirred for 10 min. Then $H_2O_2$ (30%, 40 mL) was added to the mixture and continuously stirred for 1 h. The mixture was filtered and washed with 10% HCl and 1% $H_2O_2$ solutions until the pH value was greater than 4. As synthesized graphite oxide was dispersed in deionized, 2 mg $mL^{-1}$ graphite oxide suspension was exfoliated by high power ultrasonication for 30 min.

### *2.3 Preparation of graphene sheets*

The yellowish-brown GO solution (2 mg $mL^{-1}$) was transferred to high pressure Teflon vessels of the microwave reaction system (Anton Paar Synthos 3000). The system power, temperature, pressure and reaction time were 1000 W, 200 ℃, 20 bar and 60 min, respectively. The black product was cleaned several times by centrifugation with ethanol and deionized water.

### *2.4 Characterization of samples*

The structure and morphology of the samples were characterized by scanning electron microscope (SEM, Quanta 200F), transmission electron microscopy (TEM, FEI TECNAI G2 F20) and X-ray diffraction (XRD, Bruker D8 Advance with Cu Kα radiation) operated at 40 kV and 40 mA. Raman scattering spectra (Raman, Renishaw RM-1000) were recorded in a plus laser Raman spectrometer with an excitation laser beam wavelength of 514.5 nm. Fourier transform infrared (FTIR) analysis was carried out using pressed KBr disks in the range 4000-400 $cm^{-1}$ with a PerkinElmer spectrometer. X-ray photoelectron spectroscopy (XPS, VG Scientific ESCALAB 2201XL) was carried out using Al Kα X-ray radiation and fixed analyzer transmission mode.

*2.5 Electrochemical measurements*

The electrochemical measurements were carried out using CR2025 coin-type cells. The working electrode was prepared by coating slurries consisting of active material, PVDF (polyvinylidene fluoride) and acetylene black with a weight ratio of 80:10:10 in NMP (N-methyl-pyrrolidone) solvent. The slurries was uniformly pasted on a copper foil and formed thin film, then dried at 120 ℃ in a vacuum oven for 12 h. The thin film on copper foil was cut into round disks with diameter of 12 mm and pressed under a pressure of approximately 200 kg $cm^{-2}$. Then dried at 120 ℃ in a vacuum oven for 3 h and used as anodes for the coin cells. The coin cells were assembled inside a glove box filled with pure argon, using lithium metal as the counter/reference electrode and Celgard2325 as the separator. The electrolyte was 1 M $LiPF_6$ dissolved in a mixture of dimethyl carbonate (DMC), diethyl carbonate (DEC) and ethylene carbonate (EC) (1:1:1 by weight). The galvanostatic charge-discharge curves of the cells were recorded by a Battery Testing System (Neware Electronic Co., China) at various current densities from 100 to 1000 mA h $g^{-1}$ with the voltage between 3.0 and 0.01 V *versus* $Li^+$/Li at room temperature. The cyclic voltammetry (CV) curves were measured from 0.01 to 3.0 V at a scanning rate of 0.1 mV $s^{-1}$, and electrochemical impedance spectroscopies (EIS) were obtained by applying an AC voltage of 5 mV in the frequency range of 0.01-100 kHz using an electrochemistry working station (AUTOLAB PGSTAT302).

## 3. RESULTS AND DISCUSSION

*3.1 Characterization of morphology and structure*

Fig. 1 (a) and (b) show SEM images of expanded graphite. The worm-like expanded graphite has some burls on body and is composed of many adhesion flake graphite layers, which reveals the original graphite material is already exfoliated into folded layers. And there is a large amount of free space between the folded layers, which is favorable to increase the contact area between flake graphite layers and oxidant, and improve the efficiency of oxidation, the degree of oxidation and stripping of graphite oxide. Fig. 1 (c) and (d) present the SEM images of graphite oxide, showing the layered platelets are composed of curled and wrinkled graphene sheets. It is obvious that the graphene sheets are agglomerated and overlapped. Fig. 1 (e) and (f) show that the graphene sheets are composed of thinner transparent sheets, the area of sheets is larger, and there are many folds. The transparency likes a piece of gauze and implies that the graphene sheets are only a few layers. Fig. 1 (g) shows HRTEM image of the interlayer graphene distances of edge regions, the interlayer spacing of the (002) planes is carefully measured to be 0.370 and 0.357 nm at different area, which is larger than that of graphite (0.34 nm). It is reasonable to believe that the larger interlayer distances will facilitate to accommodate lithium cations. From the electron diffraction pattern in Fig. 1 (h) and inset, it can be concluded that graphene sheets are composed of disordered and overlapped crystalline structure.

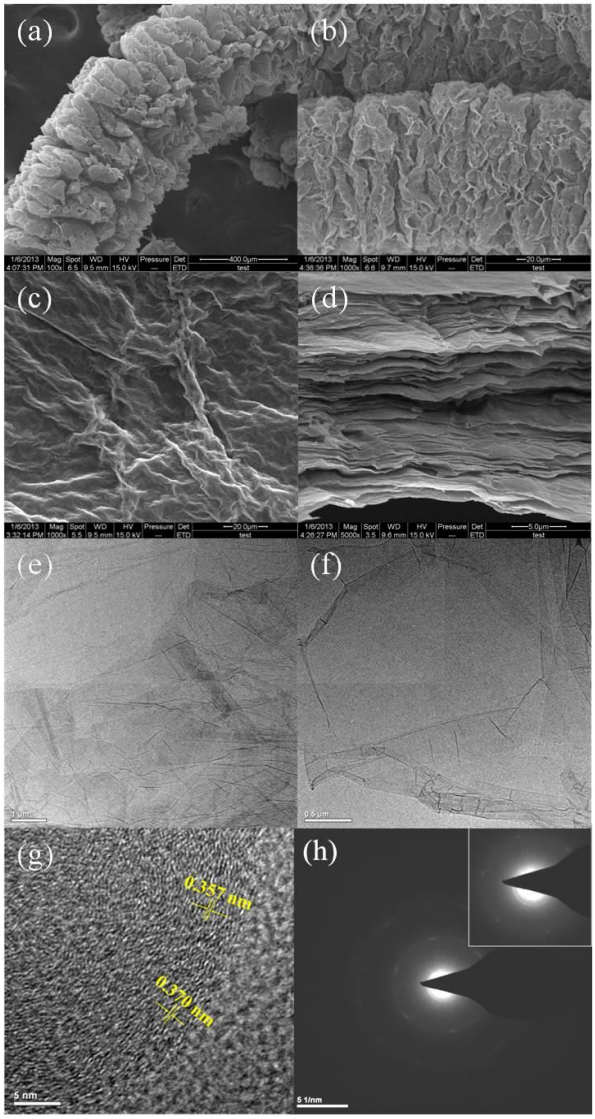


**Figure 1.** SEM images of (a) (b) expanded graphite, (c) (d) graphite oxide, TEM images of (e) (f) graphene sheets, HRTEM image of (g) graphene sheets and (h) electron diffraction patterns.

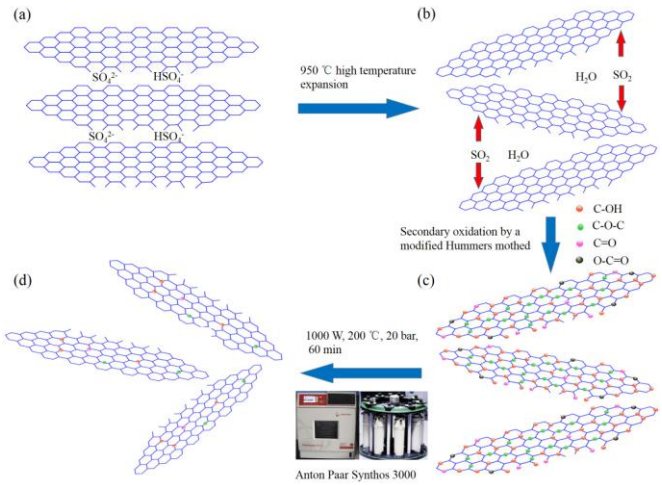


**Figure 2.** Schematic representation of the fabrication process of graphene sheets: (a) expandable graphite, (b) expanded graphite, (c) graphite oxide and (d) graphene sheets.

From the above SEM and TEM images, schematic illustrations are presented for the formation of graphene sheets, as shown in Fig. 2. The expandable graphite is prepared first using large flake graphite as raw material, many sulfate radicals and hydrogen sulfate roots enter the graphite layers and form graphite intercalated compounds. The sulfate radicals and hydrogen sulfate roots gasify and generate sulfur dioxides and vapours under high temperature. The release of sulfur dioxides and vapours damage van der Waals force between graphite interlayer, which leads to the adjacent flake graphite layer happen inhomogeneous deformation and layer spacing becomes larger. The graphite oxide is prepared by modified Hummers method. The larger layer spacing can improve the efficiency of oxidation, the degree of oxidation and stripping of graphite oxide. There are plenty of oxygen containing functional groups on the surface and edge of graphite sheets. Under high temperature and high pressure, functional groups on the surface of the graphene oxide are effectively reduced, and the reduction degree of graphene sheets is further improved. In sealed high pressure Teflon vessels of the microwave reaction system, when microwave radiates graphene oxide solution, graphene oxide and water molecules transform their orientation quickly with the microwave frequency. The total energy of the molecules is increased due to molecules rotate back and forth and collisions of friction. In addition, ion and hydrated ion of graphene oxide solution transfer back and forth and strike with adjacent molecules under the function of electric field force. Therefore the solvent can be brought to a temperature well above its boiling point by the increase of pressure resulting from heating. In this reaction, overheated supercritical water can play the role of reducing agent and offers a green chemistry alternative to organic solvents. In addition, its physiochemical properties can be widely changed with changes in high pressure and high temperature, which allows the catalysis of a variety of heterolytic (ionic) bond cleavage reactions in water [36]. The microwave digestion can reduce the reaction activation energy and change reaction kinetics, so graphene oxide is reduced easily and the reductive degree is more thoroughly.

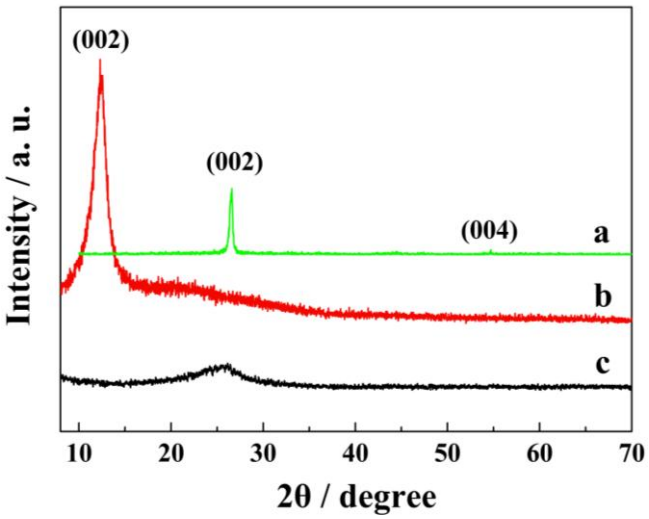


**Figure 3.** XRD patterns of (a) expanded graphite, (b) graphite oxide and (c) graphene sheets.

The X-ray diffraction patterns of the prepared products are presented in Fig. 3. The diffraction peaks of expanded graphite exhibits a characteristic peak at ~26°similar to graphite, which demonstrates that expanded graphite is still hold the structure characteristics of graphite. After oxidation, the (002) peak of expanded graphite disappears, the graphite oxide shows the (002) peak at ~12° due to the oxide-in functionalized O-groups and inserted $H_2O$ molecules [37]. These results suggest that the expanded graphite has been completely oxidized. The peak of graphene sheets is shifted back close to the expanded graphite (at ~26°) with a much broader diffraction pattern. As the concentration of O-groups is decreased during the reduction process, the material presents a larger distribution of interlayer distances which can be thought of as combinations of single layer and multilayer of graphene sheets with the O-group defects [27].

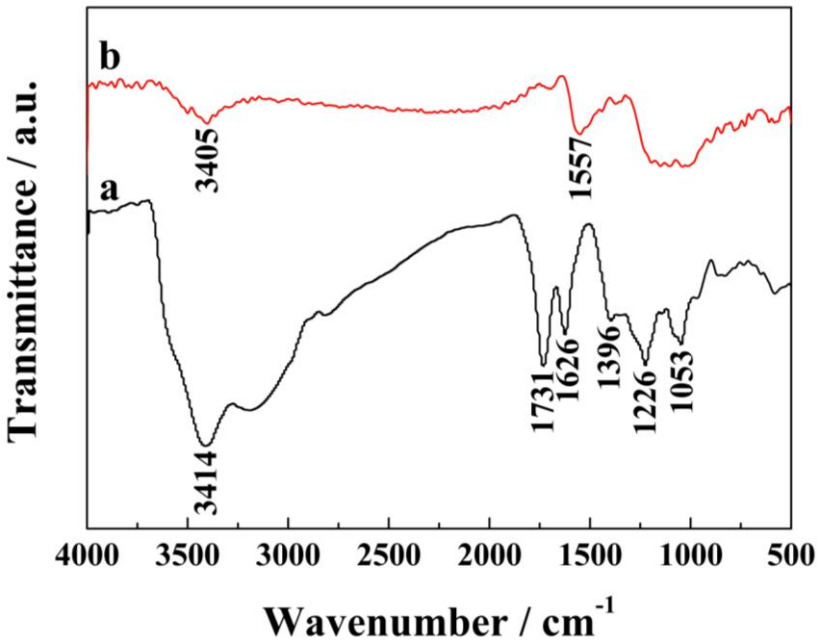


**Figure 4.** FTIR spectra of (a) graphite oxide and (b) graphene sheets.

Fig. 4 shows the FTIR spectra of graphite oxide and graphene sheets. Graphite oxide exhibits characteristic peaks at around 1731 (C=O stretching vibrations from carbonyl and carboxylic groups), 1626 (C=C skeletal vibrations), 1396 (O–H deformation vibrations), 1226 and 1053 $cm^{-1}$ (C-O stretching vibrations). Additionally, the broad peak at 3414 $cm^{-1}$ is attributed to O-H stretching vibrations of adsorbed water molecules and structural -OH groups. For the graphene sheets, the carbonyl, hydroxyl, carboxyl and epoxy groups disappeared. The peak of the broad peak at 1557 $cm^{-1}$ is attributed to skeletal vibrations of the graphene sheets. A weak signal for the C–OH stretching vibration at 3405 $cm^{-1}$ can be ascribed to the vibrations of the adsorbed water molecules. So it can be concluded that graphite oxide is reduced by the microwave digestion method.

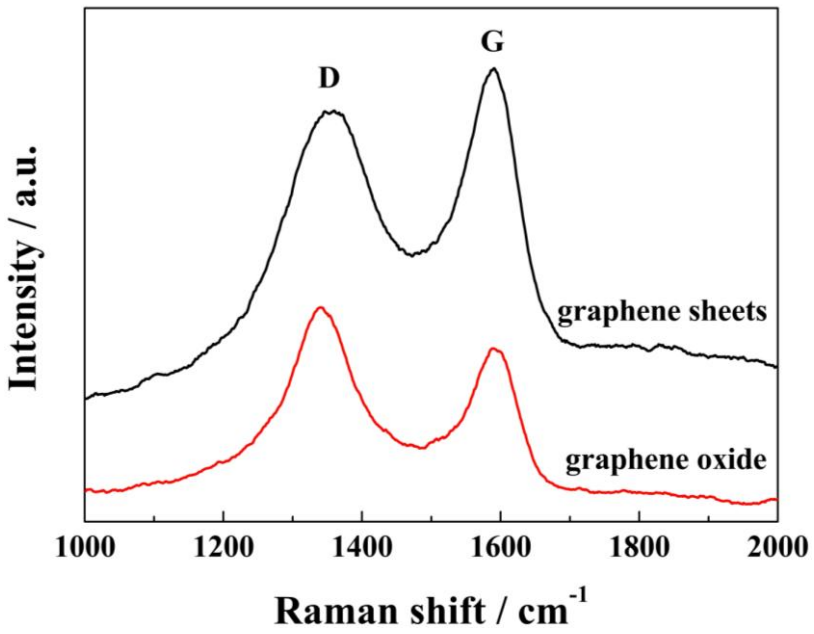


**Figure 5.** Raman spectra of graphene oxide and graphene sheets.

The Raman spectra of graphene oxide and graphene sheets are shown in Fig. 5. The peak at approximately 1590 $cm^{-1}$ is the Raman active G band originating from the $E_{2g}$ mode of graphite, which is related to the vibration of $sp^2$-bonded carbon atoms in a 2-dimensional hexagonal lattice. The peak at approximately 1346 $cm^{-1}$ is assigned to the presence to the disorder-induced D band, which is an indication of defects associated with vacancies, grain boundaries and amorphous carbon species [38]. Raman spectra with characteristic G and D bands are sensitive to defects, disorder and carbon grain size, and have been used extensively in the characterization of carbon materials. Usually, $I_D/I_G$ is a measure of disordered carbon, as expressed by the $sp^3/sp^2$ carbon ratio and an increase of $I_D/I_G$ means the degradation of crystallinity of graphitic materials [39]. From Fig. 5, the $I_D/I_G$ of graphene oxide (1.1639) is obviously higher than that of the graphene sheets (0.8924), indicating that there are many functional groups on graphene oxide sheets and more defects or disorders in the graphene oxide, and the functional groups and defects decrease after reduction reaction.

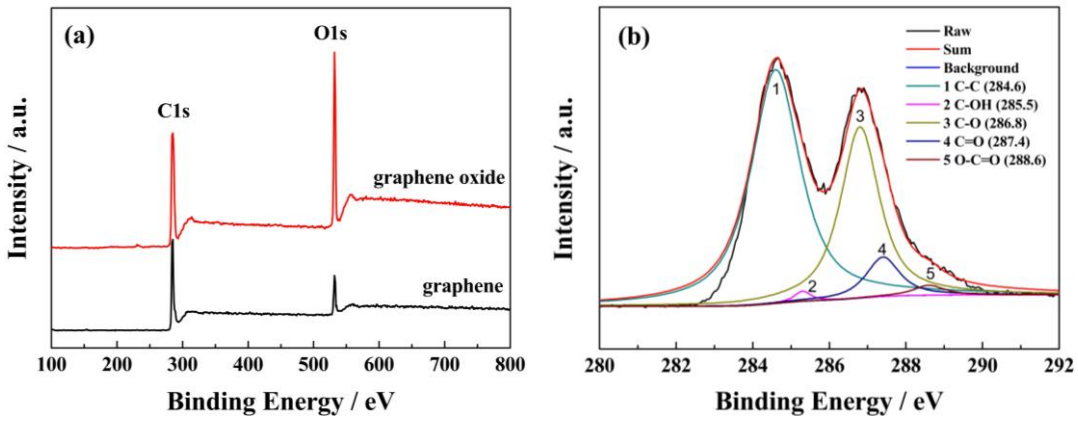

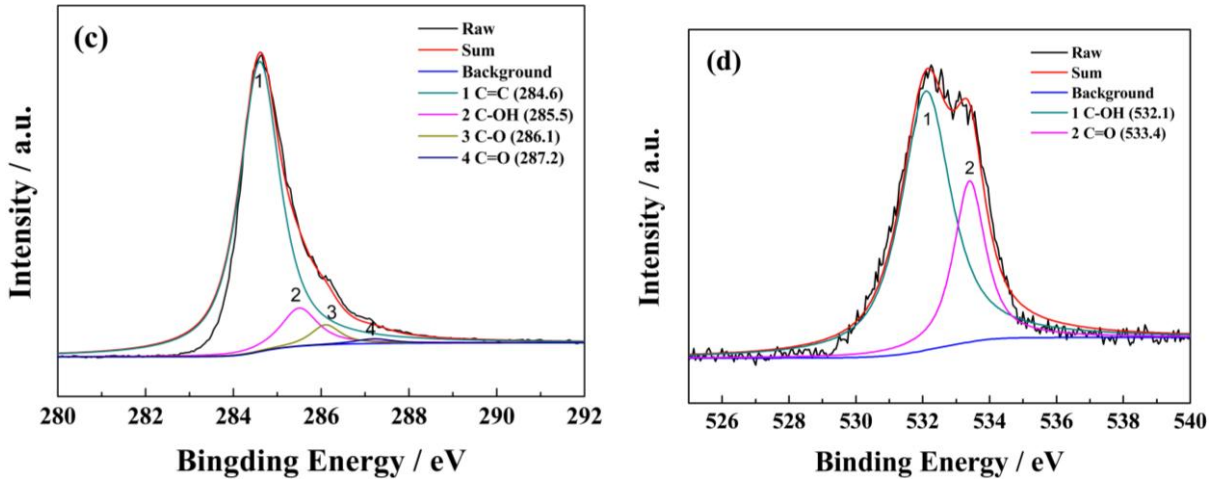


**Figure 6.** XPS spectra of (a) broad spectra of graphite oxide and graphene sheets, (b) C1s spectra of graphite oxide, (c) C1s spectra of graphene sheets and (d) O1s spectra of graphene sheets.

The reduction extent of graphite oxide is evaluated based on XPS spectra. Fig. 6 (a) shows oxygen content decreases from ~28.81% for graphite oxide to ~10.5% for graphene sheets. Fig. 6 (b) shows XPS spectra in the C1s binding energy of graphite oxide. The C1s region of graphite oxide gives five components at around 284.6, 285.5, 286.8, 287.4 and 288.6 eV, which can be generally assigned to the C-C, C-OH, C-O, C=O and O-C=O components, respectively [32]. In contrast, graphene sheets exhibits dramatically decreased intensities of the C1s components associated with carbon-oxygen bond (Fig. 6 (c)), which reveals that most of the oxygen-containing functional groups have been removed and the majority of the conjugated graphene sheets are restored after the reaction. The O1s spectrum of graphene sheets is shown in Fig. 6 (d). It consists of two peaks at 532.1 and 533.4 eV, which can be assigned to bulk $O_2$ and –OH adsorbed on the surface of graphene sheets, respectively [40]. The XRD, Raman, FIRT and XPS spectra clearly demonstrate that graphene sheets are successfully synthesized by a simple microwave digestion reduced method.

*3.2 Electrochemical performances*

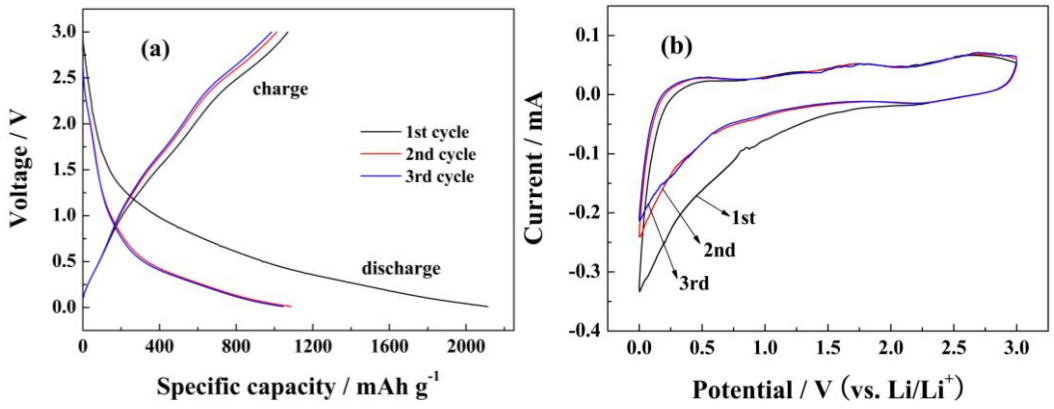

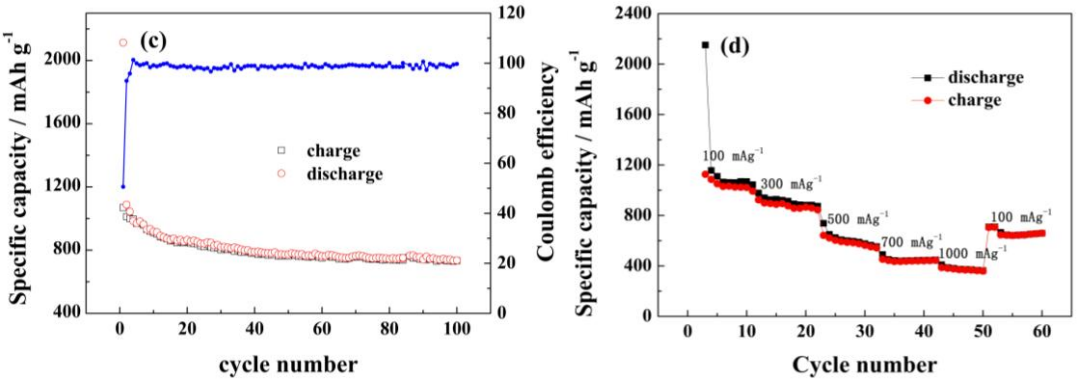


**Figure 7.** Electrochemical performance of graphene sheets. (a) First three charge/discharge profiles at the current density of 100 mA $g^{-1}$. (b) The cyclic voltammetry (CV) curves of first three cycles from 0.01 to 3.0 V at a scanning rate of 0.1 mV $s^{-1}$. (c) The cycling performances and coulomb efficiency at 100 mA $g^{-1}$. (d) The rate performance at various current densities from 100 to 1000 mA $g^{-1}$ in every 10 cycles.

The first three discharge/charge profiles of the graphene sheets at the current density of 100 mA $g^{-1}$ are shown in Fig. 7 (a). In the first cycle, the discharge and charge capacities at 100 mA $g^{-1}$ are about 2114 and 1069 mA h $g^{-1}$, respectively. The presence of the plateau at about 0.75 V in the first cycle can be attributed to the formation of a solid electrolyte interface (SEI) film on the surface of graphene sheets electrode and the reaction of lithium ion with residual oxygen-containing functional groups [41]. Because of this irreversible reaction, as well as the SEI film formed on anodes, the discharge capacity reduces to 1069 mA h $g^{-1}$, but gradually stable performance as the stability of the SEI film. The CV curves of first three cycles are shown in Fig. 7 (b). The graphene sheets anode shows an irreversible oxidation reaction at the first cycle, which is consistent with a large initial irreversible capacity during discharge/charge processes. A pronounced cathodic peak is observed at about 0.01 V, which corresponds to lithium ion insertion in graphene sheets, while there is no anodic peak occurs in the reverse cycle. It indicates that the mechanisms of lithium in this low-voltage area can be envisaged to the lithium adsorption on the graphene sheets and/or active sites [32]. An unconspicuous cathodic peak at about 0.75 V can be attributed to the formation of the SEI film on the electrode surface and the reaction of lithium ions with residual-oxygen-containing functional groups. In the following cycles, the CV curves show good repeatability, indicating that the lithium ions can reversibly reacted with the graphene sheets. The cycling performances and coulomb efficiency of graphene sheets at 100 mA $g^{-1}$ are shown in Fig. 7 (c). The discharge specific capacity at the current of 100 mA $g^{-1}$ is 733 mA h $g^{-1}$ after 100 cycles. The first coulomb efficiency is 50.56%, and then ~99.59% in the following cycles. Fig. 7 (d) shows the rate performance of graphene sheets at various current densities from 100 to 1000 mA $g^{-1}$ in every 10 cycles. The graphene sheets electrode exhibits reversible capacities of about 992, 859, 551, 442 and 356 mAh $g^{-1}$ at 100, 300, 500, 700 and 1000 mA $g^{-1}$, respectively. Additionally, when the current density reduced to 100 mA $g^{-1}$ after completed charge/discharge at different rates, the specific capacity can increase back to 713 mAh $g^{-1}$.

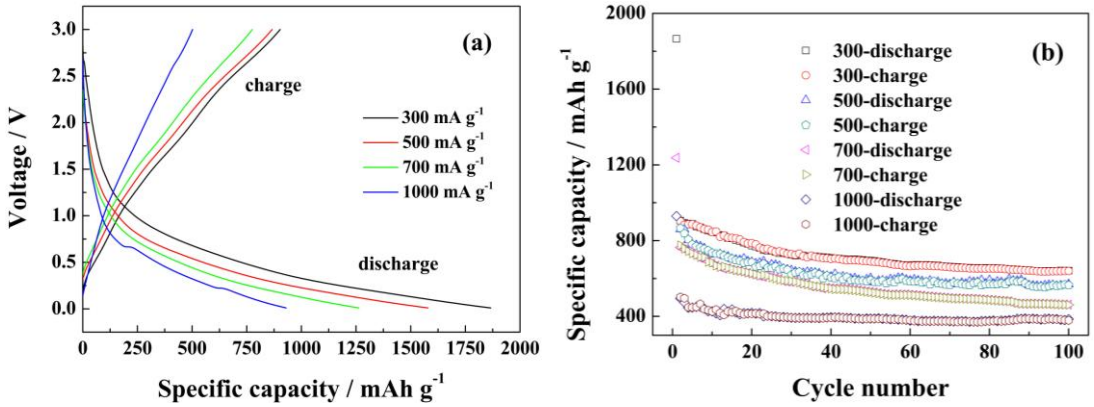


**Figure 8.** The charge/discharge profiles at large current densities. (a) First charge/discharge profiles at the current density of 300, 500, 700 and 1000 mA $g^{-1}$. (b) The cycling performances at 100, 300, 500 and 1000 mA $g^{-1}$.

From Fig. 8, we can see that the graphene sheets electrode shows excellent lithium storage properties at large current densities. The first discharge/charge profiles at the current density of 300, 500, 700 and 1000 mA $g^{-1}$ are 1865/902, 1578/865, 1237/775 and 929/502 mA h $g^{-1}$. The reversible capacities are 639, 565, 460 and 378 mAh $g^{-1}$ at 300, 500, 700 and 1000 mA $g^{-1}$ after 100 cycles, respectively.

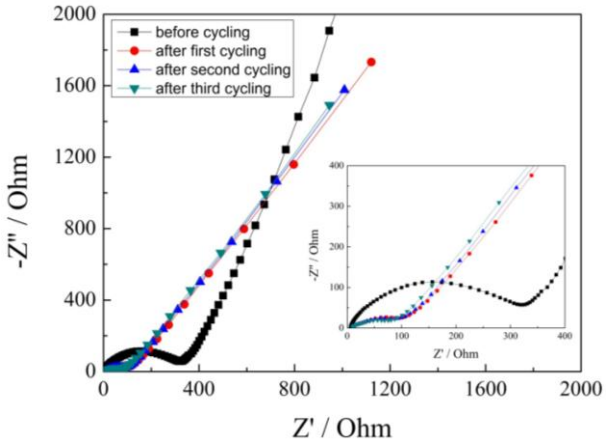


**Figure 9.** The electrochemical impedance spectra (EIS) of graphene sheets by applying an AC voltage of 5 mV in the frequency range of 0.01-100 kHz. Inset: partial enlarged detail.

The resistance of the graphene sheets electrode is analyzed by impedance analysis. Fig. 9 shows the EIS of graphene sheets at different charge/discharge cycling at the current of 100 mA $g^{-1}$. Both the spectra are comprised of a semicircle at the high to medium frequency region, followed by an inclined line ate approximately 45° to the real axis. The semicircles are related to the charge-transfer resistance and contact resistance. The inclined lines are associated with Warburg impedance corresponding to the lithium-diffusion process. The diameters of the semicircle become smaller

evidently after one cycle, indicating that the first cycle is the electrode activation process. The impedance value of graphene sheets electrode decreases in this process. The transport channel of ions and electrons in the battery system has not been established before charge/discharge. In addition, the concentration of electrode surface polarization is big. As a result, the charge-transfer resistance is bigger than that of after charge and discharge. The charge-transfer resistance decreases as the battery charge and discharge, the decreased resistance indicated enhanced ionic conductivity in graphene sheets, which is beneficial for $Li^+$ insertion/extraction into the anodes [42].

## 4. CONCLUSIONS

Few-layer graphene sheets have been successfully prepared by a microwave digestion reduced graphene oxide method using expanded graphite as raw material. The method is quick heat, easily controlled pressure and temperature, high yield rate, without any auxiliary reagents. Particularly, the graphene oxide is not must be washed to neutral. The graphene sheets are composed of thinner transparent sheets, the area of sheets is larger, and there are many folds. As anode materials in lithium ion batteries, the graphene sheets exhibits larger reversible capacity and excellent electrochemical performance. Our work demonstrates a novel approach for large-scale production of few-layer graphene materials, and realizes the production of high performance anode materials through high-efficient utilization of expanded graphite.

ACKNOWLEDGEMENT
The work is supported by National Science and Technology Support Project (no. 2013BAE04B03), Science Youth Fund in Heilongjiang Province (no. QC2013C010), and Science and Technology Research Project of the Heilongjiang Province Department of Education (no. 12531587).

## References

1. A.K. Geim and K.S. Novoselov, *Nat Mater*, 6 (2007) 183.
2. A.K. Geim, Nature, 324 (2009) 1530.
3. C.T.J. Low, F.C. Walsh, M.H. Charkrabarti, M.A. Hashim and M.A. Hussain, *Carbon*, 54 (2013) 1.
4. A.A. Balandin, S. Ghosh, W. Bao, I. Calizo, D. Teweldebrhan and F. Miao, *Nano Lett*, 8 (2008) 902.
5. C. Mattevi, G. Eda, S. Agonli, S. Miller, K.A. Mkhoyan and M. Ghhowalla, *Adv Funct Mater*, 19 (2009) 2577.
6. F.N. Xia, D.B. Farmer, Y.M. Lin and P. Avouris, *Nano Lett*, 10 (2010) 715.
7. H.I. Joh, S. Lee, T.W. Kim, S.Y. Hwang and J.R. Hahn, *Carbon*, 55 (2013) 299.
8. X. Dong, Y. Shi, W. Huang, P. Chen and L.J. Li, *Adv Mater*, 22 (2010) 1649.
9. G. Singh, A. Choudhary, D. Haranath, A.G. Joshi, N. Singh and S. Singh, *Carbon*, 50 (2012) 385.
10. J.H. Jung, J.H. Jeon, V. Sridhar and I.K. Oh, *Carbon*, 49 (2011) 1279.
11. X.Y. Peng, X.X. Liu, D. Diamond and K.T. Lau, *Carbon*, 49 (2011) 3488.
12. D.W. Zhang, X.D. Li, H.B. Li, S. Chen, Z. Sun and X.J. Yin, *Carbon*, 49 (2011) 5382.
13. N. Xiao, X. Dong, L. Song, D. Liu, Y. Tay and S. Wu, *ACS Nano*, 5 (2011) 2749.

14. F.Y. Ban, S.R. Majid, N.M. Huang, H.N. Lim. *Int. J. Electrochem. Sci*., 7(2012)4345-4351.
15. V. Sridhar, I. Lee, H.S. Yoon, H.H. Chun and H. Park, *Carbon*, 61 (2013) 633.
16. K.S. Novoselov, A.K. Geim, S.V. Morozov, D. Jiang, Y. Zhang and S.V. Dubonos, *Science*, 306 (2004) 666.
17. B. Luo, S.M. Liu and L.J. Zhi, Small, 8 (2012) 630.
18. Y. Hernandez, V. Nicolosi, M. Lotya, F.M. Blighe, Z.Y. Sun and S. De, *Nat Nanotechnol*, 3 (2008) 563.
19. S.F. Pei and H.-M. Cheng, Carbon, 50 (2012) 3210.
20. X.S. Li, W.W. Cai, J.H. An, S. Kim, J. Nah and D.X. Yang, *Science*, 324 (2009) 1312.
21. M. Lotya, Y. Hernandez, P.J. King, R.J. Smith, V. Nicolosi and L.S. Karlsson, *J Am Chem Soc*,131 (2009) 3611.
22. E. Rollings, G.H. Gweon, S.Y. Zhou, B.S. Mun, J.L. McChesney and B.S. Hussain, *J Phys Chem Solids*, 67 (2006) 2172.
23. C. Zhang, W. Lv, X.Y. Xie, D. Tang, C. Liu and Q.-H. Yang, *Carbon*, 62 (2013) 11.
24. Z.L. Wang, D. Xu, Y. Huang, Z. Wu, L.M. Wang and X.B. Zhang, *Chem Commun*, 48 (2012) 976.
25. M.S. Xu, T. Liang, M.M. Shi and H.Z. Chen, *Chem Rev*, 113 (2013) 3766.
26. J.N. Israelachvile, *Academic Press*, pp (2011) 107.
27. C. Uthaisar, V. Barone and B. Fahlman, *Carbon*, 61 (2013) 558.
28. L.J. Zhi and K. Müllen, *J Mater Chem*, 18 (2008) 1472.
29. Y. Si and T. Samulski, *Nano Lett*, 8 (2008) 1679.
30. G.X. Wang, J. Yang, J. Park, X.L. Gou, B. Wang and H. Liu, *J Phys Chem* C,C 112 (2008) 8192.
31. J.L. Zhang, H.J. Yang, G.X. Shen, P. Cheng, J.Y. Zhang and S.W. Guo, *Chem Commun*, 46 (2010) 1112.
32. Y.X. Wang, S.L. Chou, H.K. Liu and S.X. Dou, *Carbon*, 57 (2013) 202.
33. G. Demazeau, *J Mater Chem*, 9 (1999) 15.
34. M.A. Vadivel, T. Muraliganth, A. Manthiram, *Chem Mater*, 21 (2009) 5004.
35. I. Janowska, K. Chizari, O. Ersen, S. Zafeiratos, D. Soubane, V.D. Costa, et al, *Nano Res*, 3 (2010) 126.
36. M. Hassan, V. Abdelsayed, A. Khder, K.M. AbouZeid, J. Terner, M. Samy El-Shall, et al, *J Mater Chem*, 19 (2009) 3832.
37. D. Pan, S. Wang, B. Zhao, M. Wu, H. Zhang and Y. Wang, *Chem Mater*, 21 (2009) 3136.
38. E. Yoo, J. Kim, E. Hosono, H. Zhou, T. Kudo and I. Honma, *Nano Lett*, 8 (2008) 2277.
39. M.M. Lucchese, F. Stavale, E.H.M. Ferreira, C. Vilani, M.V.O. Moutinho and R.B. Capaz, *Carbon*, 48 (2010) 1592.
40. V. Sridhar, I. Lee, H.S. Yoon, H.H. Chun and H. Park, *Carbon*, 61 (2013) 633.
41. D.D Cai, S.Q. Wang, P.C. Lian, X.F. Zhu, D.D. Li and W.S. Yang, *Electrochimica Acta*, 90 (2013) 492.
42. Y. Yang, R. Pang, X. Zhou, Y. Zhang, H. Wu and S. Guo, *J Mater Chem*, 22 (2012) 23194.